The histone methyltransferase DOT1L regulates chromatin reorganization and gene expression during the postmeiotic differentiation of male germ cells

Mélina Blanco, Laila El Khattabi, Clara Gobé, Marion Crespo, Manon Coulée, Alberto de la Iglesia, Côme Ialy-Radio, Clementine Lapoujade, Maëlle Givelet, Marion Delessard, et al.

The histone methyltransferase DOT1L regulates chromatin reorganization and gene expression during the postmeiotic differentiation of male germ cells

Mélina Blanco[1], Laila El Khattabi[1,2*], Clara Gobé[1*], Marion Crespo[3], Manon Coulée[1], Alberto de la Iglesia[4], Côme Ialy-Radio[1], Clementine Lapoujade[5], Maëlle Givelet[5], Marion Delessard[1], Ivan Seller-Corona[1] , Kosuke Yamaguchi[7], Nadège Vernet[8], Fred Van Leeuwen[9], Alban Lermine[10], Yuki Okada[7], Romain Daveau[10], Rafael Oliva[4,11], Pierre Fouchet[5], Ahmed Ziyyat[1,12], Delphine Pflieger[3], and Julie Cocquet[1,13]

1 Université Paris Cité, INSERM, CNRS, Institut Cochin, F-75014 Paris, France.

2 Department of Cytogenetics, APHP.centre - Université Paris Cité, Hôpital Cochin, F-75014 Paris, France.

3 Univ. Grenoble Alpes, INSERM, CEA, UMR BioSanté U1292, CNRS, CEA, FR2048, F-38000, Grenoble, France

4 Molecular Biology of Reproduction and Development Research Group, Department of Biomedical Sciences, Faculty of Medicine and Health Sciences, Institut d'Investigacions Biomèdiques August Pi I Sunyer (IDIBAPS), Fundació Clínic per a la Recerca Biomèdica, Universitat de Barcelona (UB), Barcelona, Spain.

5 Université de Paris and Université Paris-Saclay, iRCM/IBFJ CEA, UMR Stabilité Génétique Cellules Souches et Radiations, Laboratoire des Cellules Souches Germinales, F-92265, Fontenay-aux-Roses, France

6 3P5 platform, Université de Paris, Institut Cochin, INSERM, CNRS, F-75014 Paris, France.

7 Institute for Quantitative Biosciences, The University of Tokyo, Tokyo 113-0032, Japan

8 Institut de Génétique et de Biologie Moléculaire et Cellulaire (IGBMC), Département de Génétique Fonctionnelle et Cancer, CNRS, INSERM, Université de Strasbourg, 1 rue Laurent Fries, F-67404 Illkirch, France.

9 Division of Gene Regulation, Netherlands Cancer Institute, 1066CX, Amsterdam, The Netherlands.

10 MOABI-APHP Bioinformatics Platform-I&D-DSI, Assistance Publique-Hôpitaux de Paris, Paris, France

11 Biochemistry and Molecular Genetics Service, Clinic Barcelona, Spain.

12 Service d'Histologie, d'Embryologie, Biologie de la Reproduction, AP-HP, Hôpital Cochin, F-75014 Paris, France.

13 Lead contact. Correspondence: julie.cocquet@inserm.fr

*equal contribution

Abstract

Spermatozoa have a unique genome organization: their chromatin is almost completely devoid of histones and is formed instead of protamines which confer a higher level of compaction than nucleosomes and preserve paternal genome integrity until fertilization. Histone-to-protamine transition takes place in postmeiotic male germ cells called spermatids, and is indispensable for the production of functional spermatozoa and thus for male fertility. Here we show that the H3K79 (histone 3 lysine 79) methyltransferase DOT1L controls spermatid chromatin remodelling and subsequent reorganization and compaction of spermatozoon genome. Using a mouse model in which *Dot1l* is knocked-out in adult male germ cells, we found that the chromatin of *Dot1l*-knockout (KO) spermatozoa is less compact and characterized by a higher level of retained histones and of immature forms of protamine 2. Proteomic analyses performed on differentiating male germ cells reveal that *Dot1l* KO extensively modifies the spermatid chromatin prior to histone removal. By transcriptomics, we also show that *Dot1l* KO deregulates the expression of ~1500 genes, many of which are involved in other essential aspects of spermatid differentiation such as flagellum formation. As a consequence of all these chromatin and gene expression defects, *Dot1l*-KO spermatozoa have misshapen and less compact heads, and are less motile, which results in impaired fertility.

Keywords

DOT1L, H3K79 methylation, spermatogenesis, gene regulation, histone-to-protamine replacement, chromatin compaction, flagellum development

Introduction

During the postmeiotic phase of spermatogenesis, male germ cells known as spermatids undergo profound morphological and functional changes to differentiate in spermatozoa. This process is driven by a rich genetic program characterized by the expression of thousands of genes in round spermatids (Chen et al., 2018; da Cruz et al., 2016; Ernst et al., 2019; Green et al., 2018; Soumillon et al., 2013). Then, when spermatids elongate, their chromatin is extensively remodeled which ultimately results in the eviction of ~85-99 % nuclear histones and their replacement by more basic, smaller proteins, called protamines [for reviews, see (Bao and Bedford, 2016; Rathke et al., 2014)]. This unique chromatin reorganization induces a 6-10 times higher level of compaction of the spermatozoon chromatin compared to the canonical nucleosome-based chromatin (Ward and Coffey, 1991). Non-histone packaging of male germ cell genome is conserved throughout evolution and expected to be important to protect paternal DNA from damages and prepare its reprograming in the zygote, if fertilization occurs (Rathke et al., 2014). A compact genome is also an advantage for the motile spermatozoa as it is compatible with a smaller and more hydrodynamic head (Braun, 2001).

In the past decades, the molecular mechanisms driving histone eviction and replacement have been the focus of several studies which have demonstrated the essential role of histone variants (Barral et al., 2017; Montellier et al., 2013), of histone post-translational modifications (PTMs), in particular hyperacetylation (Goudarzi et al., 2016; Oliva et al., 1987), and of writers and readers of histone acetylation (Dong et al., 2017; Gaucher et al., 2012; Luense et al., 2019; Shang et al., 2007; Shiota et al., 2018).

Interestingly, high levels of histone H3 Lysine 79 di- and tri-methylation (H3K79me2 and me3) have been observed at the same time as histone hyperacetylation, just prior to histone removal (Dottermusch-Heidel et al., 2014a; Dottermusch-Heidel et al., 2014b; Moretti et al., 2017) (Fig. 1A), but their biological significance remains to date unknown. H3K79 methylation is mediated by one enzyme, encoded by the gene *Dot1l*, of which pattern of expression and sequence are conserved from Drosophila to mammals. *Dot1l* has been implicated in development, cell reprogramming, differentiation, and proliferation [for review, see (Kim et al., 2014; Vlaming and van Leeuwen, 2016)]. It has recently been found to be essential for spermatogonial stem cell self-renewal (Lin et al., 2022) but its role in postmeiotic male germ cells, where it is the most highly expressed, has not been addressed.

In the present paper, we investigated *Dot1l* role in postmeiotic cells by a comprehensive analysis of the phenotypic and molecular consequences of its knockout in mouse male germ cells. We found that *Dot1l* is required for gene regulation and chromatin reorganization in spermatids and that its knockout leads to the production of abnormally shaped nonfunctional spermatozoa with a deficient chromatin and nucleus compaction.

Results

***Dot1l* is essential for spermatogenesis and male fertility**

In both mouse and human, *Dot1l/DOT1L* gene is highly expressed in the testis (Fig. S1A) and, more precisely, in postnatal male germ cells with a peak in postmeiotic cells, also known as spermatids (Dottermusch-Heidel et al., 2014a; Dottermusch-Heidel et al., 2014b; Moretti et al., 2017). To investigate the role of *Dot1l* in male germ cells, we generated a conditional knockout using *Stra8-Cre* recombinase (Sadate-Ngatchou et al., 2008) and a mouse transgenic line in which *Dot1l* exon 2 is flanked by LoxP sites (Jo et al., 2011) (Fig. S1B). Previous studies have reported that *Stra8-Cre* is specifically expressed in the male germline where it is expressed from post-natal day 3 and reaches maximum efficiency in pachytene spermatocytes (Bao et al., 2013; Sadate-Ngatchou et al., 2008). Bao *et al.* have also observed that *Stra8-Cre* is more efficient at cutting one allele rather than two (Bao et al., 2013). We therefore generated mice in which one allele of *Dot1l* is floxed and one allele is already deleted (Δ) to increase efficiency of floxed exon excision upon *Cre* recombinase expression (*Dot1l*$^{Fl/\Delta}$*; Stra8-Cre* mice, hereafter call *Dot1l*-KO or KO). First, to estimate the efficiency of *Dot1l* knockout, we detected DOTL1 protein by western blot and immunochemistry on adult testes from *Dot1l*-KO (*Dot1l*$^{Fl/\Delta}$*; Stra8-Cre*) and controls (*Dot1l*$^{Fl/Fl}$) (Fig. 1B, 1C, S1C and S1D). We found a reduction of >85 % of DOT1L signal but not complete abolishment/knockout of DOT1L level, despite strong activity of *Stra8-Cre* in most adult germ cells (Fig. S1E). Analyses of purified germ cell fractions confirmed reduced level but not complete absence of DOTL1 protein, along with a reduction of H3K79me2 level (Fig. 1D). Multiple protein isoforms of DOT1L have been described in the literature and several of them were observed in our western blots, including the canonical (~165 kDa) and testis-specific (~185 kDa) isoforms (Dottermusch-Heidel et al., 2014b; Zhang et al., 2004), as well as less studied isoforms such as Q679P5 (~122KDa) or Q6XZL7 (~68KDa) (https://www.uniprot.org). All of them were markedly reduced in *Dot1l*-KO testicular extracts (Fig. S1C).

To investigate the impact of *Dot1l* knockout on spermatogenesis and male fertility, the reproductive parameters of adult *Dot1l*-KO males were investigated: significant decreases in testis weight and sperm count were observed (independently of body weight, Fig. 2A, Fig. S2A and S2B). Histological analyses did not reveal a homogenous blockage/arrest at a specific stage of *Dot1l*-KO spermatogenesis, but rather the presence of “empty” tubules without germ cell or with one or more missing germ cell layer(s) (Fig. 2B and Fig. S2C). These observations were confirmed by cytometry analyses in which the number of all germ cell populations (i.e. premeiotic spermatogonia with Side Population phenotype, spermatocytes and spermatids) was found decreased in *Dot1l*-KO testes (Fig. 2C), but their frequency was not altered (Fig. S2F). Collectively, these data show that the *Dot1l* KO we produced leads to

hypospermatogenesis rather than spermatogenesis arrest. When mated to WT females, *Dot1l*-KO males were found to be hypofertile with significant reductions in the number of litters and in litter size compared to that of CTL males (Fig. 2D, S2D and S2E). In addition to *in vivo* fertility monitoring, we performed *in vitro* fertilization (IVF) assays using the same number of spermatozoa per experiment. Using spermatozoa from *Dot1l*-KO males, no oocyte was fertilized *in vitro*, while spermatozoa from control males (including WT, CTL and HET males) led to the fertilization of ~37% of oocytes (Fig. 2E. See Fig. S2G for individual values). When using oocytes devoid of zona pellucida, in order to bypass the zona pellucida crossing step, spermatozoa from *Dot1l*-KO males still performed very poorly compared to that of CTL males (~3 % of fertilized oocytes using *Dot1l*-KO sperm compared to ~88 % for CTL, Fig. 2E), confirming that *Dot1l*-KO dramatically reduces sperm fertilizing ability.

Dot1l-KO disrupts spermiogenesis and leads to the production of malformed nonfunctional spermatozoa

Our IVF data indicated that spermatozoa from *Dot1l*-KO males are less functional than those of CTL males, we therefore investigated their morphology and motility. Spermatozoa are highly specialized cells characterized by a small head which encompasses their very compact nucleus, a long flagellum that confers motility and almost no cytoplasm. First, we observed that *Dot1l*-KO epididymal spermatozoa display malformed heads and abnormal flagella (characterized by thinning of some sections in their midpiece) (Fig. 3A and Fig. S3A). Inside the flagellum, the axoneme normally contains a ring of nine outer microtubule doublets and two central microtubules (9+2 axoneme). In *Dot1l*-KO sperm, ultrastructure analyses revealed abnormal axonemes, characterized by disorganized microtubules (<9+2 microtubules) (Fig. 3B). Nuclear compaction was also found impaired, observed as less contrasted nuclei in KO in comparison with CTL sperm. *Dot1l*-KO sperm also showed an increased cytoplasmic retention (Fig. 3B and Fig. S3A). Using CASA (computer-assisted sperm analyses), we observed that *Dot1l*-KO sperm motility was impaired, with a reduced proportion of motile and progressively motile (i.e. swimming in an overall straight line or in very large circles) spermatozoa (Fig. 3C and Fig. S3B). This was not due to cell death as sperm vitality was comparable between CTL and *Dot1l*-KO mice (Fig. S3C). Axoneme/flagellum organization, nucleus compaction and cytoplasm elimination occur during the differentiation of spermatids in spermatozoa (i.e. spermiogenesis). We measured apoptosis during this transition by TUNEL assay on testicular sections, and found a higher incidence of apoptotic elongating/condensing spermatids in *Dot1l*-KO than in CTL, another indication of a defective spermiogenesis (i.e. 6% of tubules containing apoptotic elongating/condensing

spermatids in CTL vs 40% of tubules in DOT1L-KO, p =0.0007, Fig. 3D). Collectively, our data indicate that *Dot1l*-KO spermiogenesis is impaired at multiple levels and produces less functional spermatozoa.

***Dot1l*-KO extensively modifies the chromatin of postmeiotic male germ cells which results in abnormal chromatin reorganization and compaction in spermatozoa**

During spermiogenesis, spermatid chromatin undergoes specific reorganization and compaction as most histones are removed and replaced with protamines (Bao and Bedford, 2016; Rathke et al., 2014). In addition to the nuclear compaction defects observed by electron microscopy (Fig. 3B), we noticed that *Dot1l*-KO sperm chromatin is more sensitive to nucleoplasmin-induced decompaction, than CTL sperm chromatin. Nucleoplasmin, or NPM, is a histone chaperone known to facilitate paternal chromatin decompaction and reorganization after fertilization owing to its ability to bind histones and sperm nuclear basic proteins (Frehlick et al., 2007). Following NPM treatment, a higher proportion of soluble histones was found in *Dot1l*-KO compared to CTL sperm (Fig. S3D) in agreement with a nuclear/chromatin compaction defect. We next quantified residual histones in epididymal spermatozoa by western blot and found more residual histones in *Dot1l*-KO than in CTL sperm chromatin (Fig. 3E). We also quantified protamines on acid-urea gels and observed an increase in the immature (non-cleaved) forms of Protamine 2 *Dot1l*-KO spermatozoa vs. CTL (Fig. 3F). A slight but significant distorted Protamine1/Protamine2 (PRM1/PRM2) ratio was also observed in *Dot1l*-KO spermatozoa (Fig. 3F).

The transition from nucleosomes to protamine-based chromatin is the result of a complex process which starts in spermatids with the incorporation of histone post-translational modifications (PTMs) and histone variants [for reviews see (Bao and Bedford, 2016; Oliva, 2006; Rathke et al., 2014)]. To better understand how DOT1L impacts on chromatin organization prior to histone-to-protamine transition, we quantified histone PTMs and variants by liquid chromatography-tandem mass spectrometry (LC-MS/MS). In whole testis histone extracts, we observed, as expected, a clear decrease of H3K79 mono- and di-methylation (Fig. S4A) in *Dot1l*-KO samples compared to CTL (p= 0.006 and 0.005, unpaired t-test). The tri-methylation of H3K79 was not detectable with this analysis, possibly due to its small stoichiometry. No other significant differences in histone H3 PTMs were detected between *Dot1l*-KO and CTL whole testicular histone extracts. However, a significant decrease in histone H4 hyper-acetylated form (i.e. H4K5ac,K8ac,K12ac,K16ac) was observed (p= 0.02, unpaired t-test) (Fig. S4A). We next performed the same analyses on purified elongating/condensing spermatids (ES), the stages during which chromatin is extensively remodelled (Fig. 4) and on epididymal spermatozoa (Fig. S4B). In spermatozoa, some H3K79 methylation has been detected on persistent

histones (Luense et al., 2016; Moretti et al., 2017) and a significant decrease in H3K79me1 and H3K79me2 levels was visible in *Dot1l*-KO spermatozoa (Fig. S4B). In *Dot1l*-KO elongating/condensing spermatids, we also confirmed the decrease of H3K79 mono- and di-methylation (Fig. 4). Here also H3K79 tri-methylation was not detectable. Several other quantitative changes in histone H3 and H4 PTMs were observed: on both canonical H3 and variant H3.3, H3K27me2 and H3K36me2 were increased in *Dot1l*-KO elongating/condensing spermatids, with the most dramatic difference being observed for the combination K27me2K36me2. We also observed a dramatic decrease of H4K20 or R23 mono-, di- and tri-methylated forms (Fig. 4). The most remarkable change was, as in whole testes, a severe decrease in H4 acetylation in *Dot1l*-KO elongating/condensing spermatids, in particular of hyper-acetylated forms such as H4K5ac,K12ac,K16ac, H4K8ac,K12ac,K16ac and H4K5ac,K8ac,K12ac,K16ac (Fig. 4). In elongating spermatids, histone H4 hyper-acetylation is an essential step of histone-to-protamine transition, as it facilitates chromatin loosening and nucleosome disassembly prior to histone removal [for review see (Oliva, 2006)]. By western blots, we also found a decrease in H4 acetylation in *Dot1l*-KO elongating/condensing spermatids compared to CTL using anti-H4K16ac or anti-poly H4ac antibody (Fig. S4C). Finally, quantification of histone variants did not reveal striking differences between *Dot1l*-KO and CTL spermatids (Fig. S4D).

All these observations indicate that *Dot1l* KO has a profound impact on postmeiotic chromatin at the time of its reorganization which disrupts histone-to-protamine transition and leads to a higher proportion of retained histones and unprocessed protamine 2 in spermatozoa.

DOT1L regulates the expression of ~1500 genes involved in essential processes of spermatid differentiation

In order to gain insight into the gene expression changes associated with *Dot1l* deficiency in male germ cells, we performed RNA-seq analyses on purified germ cells from 3 different spermatogenic stages, each in 5 replicates: primary spermatocytes (SC), secondary spermatocytes (SCII) and round spermatids (RS) (Fig. 5A and Fig. S5A). We did not include elongating/condensing spermatids in this analysis because their transcriptome is very similar to that of round spermatids, and, at this stage, transcription progressively shuts down as a consequence of histone-to-protamine transition and genome compaction. RNA-seq differential analyses showed between 643 and 1001 deregulated genes at each stage (DEseq2, with a Fold change > 1.5 and p-value < 0.05). The number of deregulated genes increased with progression of male germ cell differentiation and was therefore highest in RS (Fig. 5B and S5B). All stages considered, 1546 genes were found deregulated, and the majority of them were found in common in at least 2 stages (i.e. 681 deregulated genes in at least 2 stages, and 285

deregulated genes in all 3 stages, Fig. 5B). We next investigated deregulated pathways using GSEA (Gene Set Enrichment Analysis) and found a downregulation of biological pathways related to apoptosis, transcription/RNA regulation, chromatin/chromosome organization and mitochondria activity in *Dot1l*-KO spermatids compared to CTL (Fig. 5C and S5C). Prior to spermiogenesis, pathways related to cilium or flagellum motor activity were found downregulated in *Dot1l*-KO primary spermatocytes while, in *Dot1l*-KO secondary spermatocytes, pathways related to chromatin/chromosome organization were the most significantly deregulated (Fig. S5C). Strikingly, 13 to 17 *Slc* genes were found deregulated in SC, SCII or RS (16 *Slc* genes significantly deregulated in *Dot1l*-KO RS, Fig. S5D). *Slc* genes encode solute carriers, and several of them have been implicated in sperm motility *via* their effects on flagellum differentiation and/or sperm energy production (Kuang et al., 2021; Maruyama et al., 2016; Toure, 2019). In agreement with the downregulation of pathways related to apoptosis, *Bcl6*, *Jak3* and *Tsc22d3* which encode proteins with anti-apoptotic effects (Aguilar et al., 2014; Kurosu et al., 2003; Thomis et al., 1997) were found significantly downregulated in RS. Finally, among the downregulated genes which are the most relevant to the chromatin reorganization defects of *Dot1l*-KO RS, we identified *Hist1h3a*, *H2afb1* and *H2afv* which encode histone H3.1 and two histone H2A variants, and the gene encoding the H3K27 demethylase KDM6A.

DISCUSSION

In the present study, using a conditional knockout mouse model, we demonstrate that the H3K79 methyltransferase DOT1L is essential for gene regulation and chromatin remodelling during spermatid differentiation.

DOT1L has been extensively studied and found to be involved in many different biological processes such as mixed lineage leukaemia (Nguyen et al., 2011; Okada et al., 2005), cell cycle (Kim et al., 2014), development (Jones et al., 2008), reprogramming (Onder et al., 2012), DNA damage repair (Lin et al., 2009; Zhu et al., 2018) or transcription activation (Steger et al., 2008; Wang et al., 2008). In the male germline, DOT1L is highly expressed in particular in postmeiotic cells (Dottermusch-Heidel et al., 2014a; Dottermusch-Heidel et al., 2014b; Moretti et al., 2017). Before meiosis, DOTL1 has been found to be required for the self-renewal of adult stem cells. Indeed, with a *Dot1l* KO induced by a Cre recombinase expressed earlier than the one used in the present study, Lin et al. observed a progressive loss of all male germ cell types (Lin et al., 2022). In the *Dot1l*-KO males we characterized here, we also found a decrease of all germ cell types, but milder, which enabled us to address the function of DOT1L in adult postmeiotic germ cells (i.e. spermatids). Strikingly, we found that *Dot1l*-KO spermatozoa

present multiple anomalies such as thinner and distorted flagella, cytoplasmic retention and impaired nuclear compaction. As a result, KO spermatozoa are less motile and their fertilizing ability is compromised. These defects are associated with the deregulation of ~1500 genes in *Dot1l*-KO meiotic and postmeiotic germ cells. Previous studies have shown that spermatid differentiation is associated with the specific expression (or highly enriched expression) of thousands of genes, and that this genetic program starts as early as in primary spermatocytes (Chen et al., 2018; da Cruz et al., 2016; Ernst et al., 2019; Green et al., 2018; Soumillon et al., 2013). Here, our analyses indicate that pathways related to "cilium/flagellum assembly or motility" are deregulated from the spermatocyte stage, and those related to "nucleosome assembly, chromatin remodelling" are deregulated in secondary spermatocytes and round spermatids (Fig. S5C). A small but significant proportion of *Dot1l*-KO spermatids undergo apoptosis and this was also visible by RNA-seq with the deregulation of "apoptosis" related pathways in RS, including the downregulation of several anti-apoptotic genes such as *Bcl6* or *Jak3* (Kurosu et al., 2003; Thomis et al., 1997). Finally, several genes encoding members of the solute carrier family were deregulated in *Dot1l*-KO male germ cells. *Slc* family members have been previously implicated in sperm motility *via* their effects on flagellar differentiation and/or sperm energy production (Kuang et al., 2021; Maruyama et al., 2016; Toure, 2019); the deregulation of *Slc* genes could therefore contribute to the sperm flagellar and motility defects of *Dot1l*-KO males. Overall, these data indicate that *Dot1l*-KO-induced gene deregulation is responsible for the multiple defects of postmeiotic male germ cell differentiation.

Spermatozoa have a unique genome organization which directly results from the replacement of most histones by protamines during spermatid differentiation. Here, we show that DOT1L controls spermatid chromatin remodelling and subsequent reorganization and compaction of spermatozoon genome. Indeed, the chromatin of *Dot1l*-KO spermatozoa is less compact, and characterized by a higher level of retained histones and of immature forms of protamine 2. Several other studies have observed a similar sperm chromatin content as a result of incomplete histone-to-protamine transition, such as *Tnp1*-KO (*transition protein 1*)(Yu et al., 2000), *H2al2*-KO (*H2A histone family member L2A*) (Barral et al., 2017), deletion of the mouse Y chromosome long arm (Yamauchi et al., 2010) or *Kat2a* – KO (aka *Gcn5)* which encodes the lysine acetyltransferase 2A (Luense et al., 2019).

In elongating spermatids, histones – in particular histone H4 – are hyper-acetylated prior to their replacement. This phenomenon is a prerequisite for histone-to-protamine transition as it creates a permissive state for histone removal [for reviews see (Bao and Bedford, 2016; Oliva, 2006; Rathke et al., 2014)]. H3K79me2/3 levels peak at the time of H4 hyperacetylation (Dottermusch-Heidel et al., 2014a; Dottermusch-Heidel et al., 2014b; Moretti et al., 2017) and we show here that both H3K79 methylation and H4 hyperacetylation are drastically reduced in *Dot1l*-KO elongating spermatids. In

other contexts than the male germline, H4 acetylation and H3K79 methylation have previously been shown to influence each other. In 2016, Gilan *et al.* showed that DOT1L-mediated H3K79me2 facilitates histone H4 acetylation (in particular of H4K5ac) and subsequent recruitment of the bromodomain-containing protein 4, BRD4, in a cell model of acute myeloid leukemia (Gilan et al., 2016). Reciprocally, in 2021, Valencia-Sanchez *et al.* showed by cryo-electron microscopy that H4K16 acetylation stimulates the H3K79 methyl transferase activity of yeast Dot1 (Valencia-Sanchez et al., 2021). In light of these data, we conclude that DOT1L-mediated H3K79 methylation is necessary for proper histone H4 hyperacetylation in elongating spermatids and for an efficient histone-to-protamine transition and compaction of the sperm chromatin.

Other changes of histone PTMs in *Dot1l*-KO elongating spermatids were observed such as increase in H3K27me2 and in H3K36 methylation (on H3 canonical histone as well as H3.3 and H3mm13 variants), and decrease in H4K20/R23 methylation. In an MLL (Mixed-lineage leukemia) model cell line, it was shown that reducing H3K36me3 by knocking down the expression of SETD2 (SET domain containing 2) enzyme results in upregulation of H3K79me2 level (Bu et al., 2018). Here, our data suggest that loss of H3K79 methylation could reciprocally lead to an increase in H3K36 methylation. Alternatively, the multiple changes in histone PTMs could be compensatory mechanisms for H3K79 methylation loss, as observed in *Th2b* knock-out male germ cells in which H2B was upregulated and several histone PTMs and variants changed to compensate for the loss of H2B variant TH2B (Montellier et al., 2013). The deregulation of genes associated to “chromatin function” could also contribute to the observed chromatin changes. This is exemplified by the increase in H3K27me2 detected in *Dot1l*-KO elongating/spermatids following the downregulation of the gene encoding the H3K27 demethylase KDM6A in round spermatids.

Finally, in light of the abnormal chromatin content and compaction observed in *Dot1l*-KO spermatozoa, it would be interesting to investigate their impact on early embryo chromatin reorganization and DNA integrity. Indeed, abnormal sperm chromatin compaction can lead to a high incidence of DNA damage which may not be all repaired by the early embryo and may lead to developmental arrest [see (Garcia-Rodriguez et al., 2018) for review]. Using a technology which consists in directly injecting a spermatozoon in the oocyte (i.e. IntraCytoplasmic Sperm Injection, ICSI), it should be possible to overcome the inability of *Dot1l*-KO sperm to *in vitro* fertilize embryos, and use this model to better understand the impact of abnormally compacted sperm on embryo chromatin and development.

Materials and methods

Mouse strains and genotyping

Conditional *Dot1l* knockout mice were obtained from the Knockout Mouse Project (CSD29070) (to F.V.D). This line has previously been described in (Jo et al., 2011). In these mice, *Dot1l* exon 2 is flanked by loxP sites (see Fig. S1B). Recombination of loxP sites by Cre recombinase leads to the deletion of exon 2 and consequently a frameshift and premature stop codon in *Dot1l* Coding DNA sequence. Tg(*Stra8-iCre*)1Reb/J were obtained from the Jackson lab (JAX stock #017490) (Sadate-Ngatchou et al., 2008). All animals analyzed in this study were from a C57BL6/J background. Genotypes of animals were determined by polymerase chain reaction (PCR) using *Dot1l* primers F+R1+R2 (Fig. S1) or *iCre* primers as described on the Jackson lab website. The latter PCR was performed with *Ymtx* internal control (see Table S1 for primer list and sequences).

Reproductive parameters were analyzed on two types of *Dot1l* knocked-out animal models. First, on animals hosted in a conventional animal house (cah) and of the following genotypes: $Dot1l^{Fl/Fl}$; *Stra8-Cre* mice (DOT1Lcah) and $Dot1l^{Fl/Fl}$ siblings (without *Stra8*-Cre transgene) as controls (CTLcah). Second, on animals hosted in a Specific Pathogen-Free (SPF) animal house and of the following genotypes: $Dot1l^{Fl/\Delta}$; *Stra8-Cre* (hereafter called DOT1L-KO) and $Dot1l^{Fl/Fl}$ siblings as controls. Analyses of the reproductive parameters of both types of KO males ($Dot1l^{Fl/Fl}$;*Stra8-Cre* or $Dot1l^{Fl/\Delta}$; *Stra8-Cre*) gave similar results (Fig. S2A and B). Heterozygous $Dot1l^{Fl/\Delta}$ males (HET) were also analyzed. They did not differ from controls (Fig. S2 A-E). $Dot1l^{Fl/\Delta}$; *Stra8-Cre* animals were generated because it had been shown that *Stra8-iCre* is not 100 % efficient (Bao et al., 2013). In these animals, one allele of *Dot1l* is floxed and one allele is already deleted (Δ) to increase the efficiency of floxed exon excision upon *Cre* recombinase expression. Nevertheless, some remaining DOTL1 protein signal was observed by Western blot and Immunofluorescence (see Fig. 1B-D and Fig. S1C and D). All other phenotypic analyses and all molecular analyses were performed on $Dot1l^{Fl/\Delta}$; *Stra8-Cre,* hereafter called *Dot1l*-KO, and on $Dot1l^{Fl/Fl}$ siblings as CTL. Unless specified, all analyses were performed on adult (~3 to 6 month-old) males. Mice from mTmG line (Muzumdar et al., 2007) were crossed to *Stra8-Cre* line to verify *Stra8-Cre* recombinase location and activity**.**

The mice were fed ad libitum with a standard diet and maintained in a temperature- and light-controlled room. Animal procedures were approved by Universite de Paris ethical committee (Comite d'Ethique pour l'Experimentation Animale; registration number CEEA34.JC.114.12, APAFIS 14214-2017072510448522v26).

Fertility tests

Dot1l-KO and CTL males, aged from 8 to 10 weeks, were housed with two wild-type C57BL6/J females per cage (aged from 6 weeks, Janvier Labs, France) for up to 4 months. Vaginal plugs were checked and females separated when found. For each group, litter size and number were assessed.

IVF

Oocyte preparation: WT C57BL6/J female mice aged 6 to 8 weeks (Janvier Labs, France) were superovulated with 5 IU of pregnant mare serum gonadotropin (PMSG) and 5 IU human chorionic gonadotropin (hCG) (Intervet, France) 48 hours apart. About 14 hours after hCG injection, animals were sacrificed by cervical dislocation. Cumulus oocyte complexes were collected by tearing the ampulla wall of the oviduct, placed in Ferticult medium (FertiPro N.V, Belgium) supplemented with 3 % BSA (Sigma–Aldrich), and maintained at 37°C under 5 % CO2 in air under mineral oil (FertiPro N.V, Belgium). When experiments were performed with Zona-free oocytes, cumulus cells were first removed by a brief exposure to hyaluronidase IV-S (1 mg/ml, Sigma–Aldrich). The zona pellucida was then dissolved with acidic Tyrode's (AT) solution (pH 2.5) (Sigma–Aldrich) under visual monitoring. Zona-free eggs were rapidly washed five times and kept at 37°C under 5 % CO2 in air for 2 to 3 hours to recover their fertilization ability.

Capacitated sperm preparation: mouse spermatozoa were obtained from the cauda epididymides of DOT1L-KO, CTL, HET and WT C57BL6/J males (aged 8 to 12 weeks) and capacitated at 37°C under 5 % CO2 for 90 minutes in a 500 µl drop of Ferticult medium supplemented with 3 % BSA, under mineral oil.

In vitro fertilization: cumulus-intact and Zona-free eggs were inseminated with capacitated spermatozoa for 3 hours in a 100 µl drop of Ferticult medium, 3 % BSA at a final concentration of 10^6 or 10^5 per ml, respectively. Then, they were washed and directly mounted in Vectashield/DAPI (Vector laboratories, CA, USA) for observation under UV light (Nikon Eclipse E600 microscope). Only oocytes showing at least one fluorescent decondensed sperm head within their cytoplasm were considered fertilized.

Germ cell purification by elutriation or FACS

Germ cells were purified from adult males using fluorescence-activated cell sorting (FACS) or elutriation as previously described in (Cocquet et al., 2009; Comptour et al., 2014) and more recently in (Crespo et al., 2020). Elutriated fractions with a purity ~95–99% for elongating/condensing spermatids were used for LC-MS/MS analyses. Highly enriched fractions of primary or secondary spermatocytes (>90%) and round spermatids (~99%) were used for RNA-Seq analyses. Flow cytometric

391 analysis of testicular cell suspension were performed as previously described (Corbineau et al., 2017;
392 Ragazzini et al., 2019).

393 **Sperm collection and purification with Percoll**

394 Spermatozoa were extracted from cauda epididymis in pre-warmed (37°C) M2 medium (Sigma-Aldrich)
395 by gentle pressure. Then, epididymides were perforated with a thin needle and incubated in M2 for
396 10 min at 37°C to allow remaining sperm to swim up. For molecular analyses, spermatozoa were next
397 purified on a Percoll gradient. In brief, spermatozoa were centrifuged at 2000 g for 10 min and pellets
398 incubated in somatic cell lysis buffer (1X PBS, 0.1% SDS, 0.5% Triton X-100) for 10 min on ice. Sperm
399 cells were washed with PBS-BSA (1X PBS, 0.5% BSA, 2mM EDTA) and briefly sonicated to remove
400 flagella (ON 5 sec – OFF 30 sec x 3 Cycles, bioruptor Pico, Diagenode). The samples were transferred in
401 low retention tubes, loaded on 50% Percoll (Sigma-Aldrich) and centrifuged at 2500 g for 5 min to
402 remove somatic cells and flagella. This step was repeated once and sperm cells were washed in PBS-
403 BSA twice and counted (minimum 1 000 cells). The purity was >99.7%. Sperm pellets were snap-frozen
404 in liquid nitrogen and stored at -80°C prior to use.

405 **Nucleoplasmin decompaction**

406 Experiments were performed as previously described in (Yamaguchi et al., 2018). Following Percoll
407 purification, sperm heads were washed in 1X PBS, 0.5% Tween, permeabilized with 0.02 U/M
408 Streptolysin O (Sigma-Aldrich) in 1X PBS for 10 min on ice and washed once with 1X PBS, 0.5% Tween.
409 Cells were then incubated with 1X PBS containing 1 mM DTT for 10 min at 37°C, washed with 1X PBS,
410 0.5% Tween, resuspended in KH buffer (100 mM KCl, 20 mM Hepes-KOH, pH 7.7) in low retention tubes
411 and stored at -80°C for later use. Ten millions of sperm heads were resuspended in 1 mL NPM
412 treatment buffer (20 mM HEPES-KOH, pH 7.7, 100 mM KCl, 2.5 mM MgCl2, 5 mM Na-But, 10 mM DTT,
413 1X complete EDTA-free protease inhibitors, 250 µM NPM) and incubated for 2 h at 37 °C in a
414 Thermomixer (Mixer HC, Starlab) at 1000 rpm. After centrifugation at 20 000 g for 5 min at 4°C, cells
415 were washed with 5 mM Na-But in 1X PBS, 0.5% Tween twice and sperm heads were fixed with 1%
416 PFA for 10 min at RT, quenched with 250 mM glycine and washed in 5 mM Na-But in PBS/Tween 0.5%
417 twice.

418 After fixation, sperm pellets were resuspended in NP40 Buffer (10 mM Tris-HCl, pH 8.0, 10 mM NaCl,
419 0.5% NP40, 1X complete EDTA-free protease inhibitors, Sigma Aldrich) and incubated on ice for 30 min.
420 Samples were washed with 1X PBS, 0.5% Tween, 5 mM Na-But, and resuspended in 200 µL of
421 sonication buffer (10 mM Tris-HCl, pH 8.0, 20% glycerol, 0.25% SDS, 5 mM Na-But, 1X complete EDTA-
422 free protease inhibitors). Sperm cells were sonicated (ON 30sec – OFF 30sec x13 cycles, Bioruptor Pico,
423 Diagenode) and the sheared chromatin was centrifuged at 20 000 x g for 10 min at 4°C. Supernatants

were transferred in new 1.5 mL tubes and pellets resuspended in 200 µL of KH buffer. Prior to western-Blot analyses, both supernatant and pellets were resuspended in 4X NuPage/10% β-mercapto-ethanol (ThermoFisher), heated 10 min at 95°C and briefly sonicated.

Histone extraction from spermatozoa

Experiments were performed as described in (Crespo et al., 2020) with minor modifications. In brief, five millions of Percoll-purified spermatozoa were incubated in 50mM DTT for 30 min (at 4°C) then mixed with sulfuric acid (0.4M final volume), sonicated and acid extracted with 20% trichloroacetic acid (TCA). Histone pellets were washed with cold acetone containing 0.05% HCl, dried at room temperature, and resuspended in 50µl of SDS-PAGE loading buffer containing 10% β-mercapto-ethanol.

Western blot

Electrophoresis was performed in polyacrylamide gels at 120 V in denaturating buffer containing 25 mM Tris Base, 190 mM glycine, 0.1 % SDS and proteins were transferred on nitrocellulose membranes (GE Healthcare). Membranes were then rinsed and incubated 3 min in Ponceau stain to visualize transfer efficiency. Then membranes were incubated in 1X PBS, 0.01 % Tween, 5 % milk. All primary antibodies were incubated over night at 4°C (see table S2 for references and dilutions) and 2 h at room temperature for secondary antibodies. The revelation was performed with SuperSignal West Pico Plus® ECL from ThermoFisher (34580) and Immobilon ECL Ultra Western HRP substrate from Millipore (WBULS0100) on ImageQuant™ LAS 4000 imager.

Extraction and analysis of protamines

P1/P2 protamine ratio was analyzed following procedures of protamine-rich fraction of sperm nuclear proteins extraction and analysis previously described, with minor modifications (Soler-Ventura et al., 2018). Briefly, histones and other basic proteins loosely attached to DNA were extracted incubating sperm in 0.5 M HCl for 10 min at 37 ºC after vortexing, and centrifuged at 2000 *g* 20 min at 4 ºC. This step was repeated three times. Resulting pellet was resuspended in 0.5 % Triton X-100, 20 mM Tris-HCl (pH 8), and 2 mM $MgCl_2$. After centrifugation at 8940 *g* 5 min at 4 ºC, the sediment was resuspsended in milliQ H_2O with 1 mM PMSF, centrifuging again at the same conditions. Chromatin was then denaturated by resuspending the pellets in 20mM EDTA, 1mM PMSF, 100mM Tris-HCl- pH8) and adding 1 volume of 575 mM DTT in 6 M GuHCl prior vortexing. The solution was incubated at 37 ºC with 0.8 % 4-vynilpyridine to inhibit cysteine disulfide bonds for 30 min, vortexing every 5 min, in fumehood and in dark conditions. Chromatin was then precipitated with a minimum of 10 min incubation with cold ethanol at -20 ºC, followed by centrifugation 12880 *g* for 15 min at 4 ºC. Basic

nuclear proteins (protamine-enriched fraction) were extracted from DNA incubating with 0.5 M HCl at 37 ºC and recovered in the supernatant after centrifugation at 17530 *g* for 10 min at 4 ºC. Precipitation was carried out with 20 % TCA on ice and centrifugation using the same conditions. Protamines were washed twice with 1 % β-mercaptoethanol in acetone and dried out at room temperature. For in-gel quantification, dried purified extracts were resuspended 5.5 M urea, 20% β-mercaptoethanol, 5% acetic acid, and separated using acetic-acid urea gel electrophoresis (AU-PAGE). Gels were stained with EZBlue™ Gel Staining Reagent (#G1041, Sigma Aldrich) and optic density of the bands corresponding to mouse PRM1 and PRM2 was quantified using Quantity One 1-D analysis software (BioRad, Hercules, CA, USA) to calculate the PRM1/PRM2 ratio. PRM1/PRM2 ratios were normalized against the control group.

Histological analyses

Mouse testes were fixed in 4 % buffered paraformaldehyde (PFA) for minimum 4 h, before they were cut in halves and incubated overnight in Bouin (Sigma). Testes were then washed in 70 % ethanol at room temperature for 30 min, dehydrated, and embedded in paraffin. Four µm-sections were stained with periodic acid–Schiff (PAS).

Immunohistochemistry and immunofluorescence

Mouse testes were fixed in 4 % buffered paraformaldehyde (PFA) for minimum 4 h, before they were cut in halves and incubated overnight in 4 % PFA. Testes were then washed in 70 % ethanol at room temperature for 30 min, dehydrated, and embedded in paraffin. Immunohistochemistry or immunofluorescence experiments were performed on 4 µm-sections using Novolink polymer detection system (7140-K, Leica Micro-systems) according to the manufacturer's instructions, or following the procedure described in (Comptour et al., 2014) with the following modifications. Permeabilization was performed for 15 min in 1X PBS, 0.5 % Triton X-100. Blocking was performed for 30 min to 1 h at room temperature in 1X PBS, 0.1 % Tween, 1 % BSA. Primary antibody was incubated overnight at 4°C (dilution and reference of each antibody are available in Table S2). Some slides were counterstained with Hematoxylin. For immunofluorescence experiments, lectin (L-21409 or L-32459, ThermoFisher) was diluted at 1/500 in 1X PBS and incubated for 1 h at room temperature along with secondary antibodies (see (Comptour et al., 2014)). Lectin was used to stain the developing acrosome and determine the stage of testis tubules as described in (Ahmed and de Rooij, 2009). DAPI (in VECTASHIELD Mounting Medium, Vectorlab) was used to stain nuclei. TUNEL assay was performed on 4 µm paraffin-embedded testicular sections using In Situ Cell Death Detection Kit, Fluorescein as described by the manufacturer (Roche, Sigma-Aldrich). GFP immunofluorescence pictures were taken with a NikonE600 microscope using the Nikon Digital Sight SD-V3 camera (DS-Fi1) with the NIS

489 software. All other immunofluorescence pictures were taken with an Olympus BX63 microscope and
490 analysed using ImageJ 1.48v (http://imagej.nih.gov/ij/). Immunohistochemistry pictures were taken
491 with Perkin Elmer Lamina slide scanner and analyzed using CaseViewer software.

492 **Papanicolaou staining of spermatozoa**

493 Spermatozoa were collected from cauda epididymides in M2 medium (Sigma-Aldrich) and spread onto
494 a Superfrost Plus slide (ThermoFisher). Cells were fixed in 4 % PFA for 10 min and stained using
495 Papanicolaou staining. Briefly, the slides were washed in 95 % ethanol, incubated in Harris hematoxylin
496 for 3 min for nucleus counterstaining, washed and stained with OG-6 dye (RAL diagnostics 05.12013,
497 Martillac, France) and with EA-50 (RAL diagnostics 05.12019, Martillac, France). The slides were then
498 dehydrated and mounted with permanent mounting medium. Spermatozoa were then observed with
499 NikonE600 optic microscope and pictures were taken with the 40X objective.

500 **Electron microscopy**

501 Ten to 20 million epidydimal spermatozoa were collected in 2ml of fresh M2 medium (Sigma-Aldrich)
502 prewarmed at 37°C. After pelleting the sperm at room temperature (300g, 10 min), the pellet was fixed
503 in 3 % glutaraldehyde for 1 h before washing twice in 1X PBS (1000g, 10 min). Samples were then
504 dehydrated in ethanol baths and incubated in propylene oxide before inclusion in gelatin. Slices of 60
505 nm were cut with a Diatome and observed with a *JEOL 1011* microscope at a magnification of 1500X
506 or 2000X. Spermatozoa from 4 CTL and 4 DOT1L-KO mice were analyzed.

507 **Computer assisted sperm motility analysis (CASA)**

508 Immediately after collection of epididymal spermatozoa in M2 medium (Sigma-Aldrich), sperm motility
509 was analyzed by computer-assisted sperm analysis (CASA) systems CASA CEROS II (Hamilton Thorne,
510 Beverly, MA, USA), using a Zeiss microscope. Sperm motility parameters from 12 CTL and 10 DOT1L-
511 KO males were collected.

512 **Sample preparation for RNA-seq**

513 Total RNA from 150,000 to 600,000 cells of sorted primary spermatocytes (SCI), secondary
514 spermatocytes (SCII) and round spermatids (RS) was extracted using the Ambion RNAqueous micro kit
515 (ThermoFisher) following manufacturers' instructions. For each cell type, 5 replicates were analyzed.
516 Quantity and quality were assessed using Bioanalyzer chips (ThermoFisher). Libraries were prepared
517 using the NEBNext Ultra II Directional RNA Library Prep Kit (New England Biolabs) according to supplier
518 recommendations. Paired-end sequencing of 100-bp reads was then carried out on the Illumina
519 HiSeq4000 system.

RNA-seq analyses

Datasets have been submitted to ENA repository under project number PRJEB50887 (https://www.ebi.ac.uk/ena/). Snakemake was used for RNA-seq analyses (Koster and Rahmann, 2018)(v. 3.9.0). Adaptors were trimmed and reads with poor quality (quality < 20) were filtered out with BBduk from BBTools (v. 38.23, https://sourceforge.net/projects/bbmap/). Alignment was performed on the mouse genome build mm10 (GRCm38.p6) using STAR (Dobin and Gingeras, 2015) (v. 2.7.2d) and Gencode vM19 gene annotation GTF with following arguments : --outMultimapperOrder Random --quantMode Genecounts --sjdbOverhang 74. For each sample, the number of aligned reads was converted in cpm (count per million). Genes with an expression level of at least > 1cpm in a minimum of 2 samples were included in the analysis, to exclude genes with a very low expression. Differential expression analysis was carried out using DESeq2 (Love et al., 2014) and edgeR (Robinson et al., 2010) packages using default parameters and a design using genotype and cell type. Differentially expressed genes (p-value<5 %) were obtained using glmTreat edgeR's function which conducts a modified likelihood ratio test (LRT) against the fold change threshold (> 1.5). This method is based on TREAT method (McCarthy and Smyth, 2009). Enrichment analysis was performed with GSEA (v. 4.0.3, c5.all.v7.1.symbols.gmt, GO cellular components, biological pathways, or all) on gene expression cpm values between KO and control samples (Subramanian et al., 2005) (Fig. S5E). Beforehand, mouse Ensembl gene ID were converted to human Ensembl gene ID (hg38) with the biomaRt R package (Durinck et al., 2005).

Code availability

The fully reproducible and documented analysis is available on github at https://github.com/ManonCoulee/RNAseq_DOT1L_Blanco_2022.

MS quantification of histone PTMs and of histone variants

To identify histone PTMs, samples were prepared and processed essentially as described in Crespo *et al.* (Crespo et al., 2020). Briefly, histones were precipitated by acid extraction from whole testes which were beforehand reduced into powder using a pestle and mortar on dry ice, or from elutriated elongating/condensing spermatids (ES). They were resuspended in loading gel buffer (LDS sample buffer reference 84788, supplemented with NuPAGE sample reducing agent reference NP0009, ThermoFisher) and separated on a 4-12% NuPAGE acrylamide gel (reference NP0321BOX, ThermoFisher). After blue staining (SimplyBlue SafeStain, ThermoFisher), gel bands corresponding to H3 and H4 were cut and then reduced with dithiothreitol, alkylated with iodoacetamide and in-gel digested with 0.1 µg trypsin (V511, Promega) per slice using a Freedom EVO150 robotic platform (Tecan Traging AG, Switzerland). Alternatively, to analyze the relative abundance of histone variants

between conditions, histone samples were simply loaded on a gel and migrated for a few mm. The whole zone was cut for robotic in-gel tryptic digestion. The resulting tryptic peptides were analyzed by a liquid chromatography-tandem mass spectrometry coupling made up of a C18 reversed-phase capillary column (75 µm i.d. x 25 cm ReproSil-Pur C18-AQ, 1.9 µm particles, Cluzeau, France) using the UltiMate™ 3000 RSLCnano system (ThermoFisher) coupled to a Q-Exactive HF mass spectrometer (ThermoFisher). The mobile phases consisted of water with 0.1% formic acid (A) and acetonitrile with 0.08% (v/v) formic acid (B). Peptides were eluted with a gradient consisting of an increase of solvent B from 2.8% to 7.5% for 7.5 min, then from 7.5% to 33.2% over 33.5 min and finally from 33.2% to 48% over 6.5 min. Mass spectrometry acquisitions were carried out by alternating one full MS scan with Orbitrap detection acquired over the mass range 300 to 1300 m/z and data-dependent MS/MS spectra on the 10 most abundant precursor ions detected in MS. The peptides were isolated for fragmentation by higher-energy collisional dissociation (HCD) with a collision energy of 27.

Identification of modified peptides was obtained using our in-house established database of histone sequences, MS_histoneDB (El Kennani et al., 2017), completed with a list of 500 common contaminants. MS/MS data interpretation was carried out with the program Mascot (http://www.matrixscience.com/) with the following search parameters. The precursor and fragment mass tolerances were 5 ppm and 25 mmu, respectively; enzyme specificity was trypsin; the maximum number of trypsin missed cleavages was set to 5, carbamidomethyl (Cys) was specified as a fixed modification. We indicated as variable PTMs in Mascot acetylation, crotonylation and ubiquitination (more precisely the dipeptide “GG”) of Lys residues, methylation and di-methylation of Lys/Arg and tri-methylation of Lys, as well as N-terminal acetylation of proteins. Filtering of peptide identifications and quantification was performed by using the program Proline (Bouyssie et al., 2020). All peptide/spectrum matches of scores below 25 were filtered out; next, all identifications of modified peptides suggested by Mascot were visually validated by demanding that a continuous stretch of minimally 5 amino acids be identified in terms of b or y fragment ions, and by ascertaining PTM positioning on Lys/Arg residues. When interpreting our mass spectrometry data against the database MS_histoneDB, we were able to identify and quantify various H3 variants, namely canonical H3 and variants H3.3, testis-specific H3t and H3mm13. H3t differs from canonical H3 at residue 24, while H3.3 and H3mm13 differ from H3 at residues 31 and 29. To estimate the relative abundance of modified histone peptides between samples, normalization to be at constant amount of total H3 or H4 was done by dividing the raw MS signals of modified peptides by the MS signals of barely modified peptides detected with high intensity, namely STELLIR for histone H3, and ISGLIYEETR and DNIQGITKPAIR for histone H4. To estimate the relative abundance of histone variants between DOT1L-KO and CTL samples, variants were quantified by Proline by relying only on peptides specific of these sequences.

Samples were normalized to be at constant amount of histone H4. The mass spectrometry proteomics data have been deposited to the ProteomeXchange Consortium via the PRIDE (Perez-Riverol et al., 2019) partner repository with the dataset identifier PXD030734 and 10.6019/PXD030734.

Statistical Analysis

Chi-square analysis was used to analyze IVF data. Sperm motility parameters were analyzed using a Mann Whitney tests following angular transformation of percentages. To compare the incidence of sperm head abnormalities, and apoptotic (TUNEL+) spermatids between *Dot1l*-KO and CTL, percentages were converted in angles prior to performing t-tests. Student t-test was also used for all other analyses (fertility, sperm count, testis weight, histology, histone PTM, western blot and PRM1/2 ratio quantifications).

Acknowledgements

We would like to thank Cochin Institute (INSERM U1016, CNRS UMR8104, Universite Paris Cité) core facilities, in particular, Alain Schmitt from the electron microscopy platform, and all the staff from the animal house, histology (HistIM), genomic (GENOM'IC), cytometry (CYBIO) and imaging (IMAG'IC) core facilities. We would also like to thank Aminata Touré and Marjorie Whitfield for advices and discussion on sperm morphology and motility analyses. M.Cr. and D.P. are grateful to their colleagues in EDyP for their support on LC-MS instruments and in informatics. This work was supported by the Agence Nationale de la Recherche (ANR-17-CE12-0004-01 to J.C.), the Fondation pour la Recherche Médicale (SPF201909009274 to C.G.) and grants from "Ministerio de Economía y competitividad" FI17/00224 to A.I., and "Ministerio de Ciencia e Innovación" PI20/00936 to R.O. and MV20/00026 to A.I. M.B and M.Co. received a PhD funding from Université Paris Cité, M. Cr., from University Grenoble Alps (UGA). The proteomic experiments were partially supported by Agence Nationale de la Recherche under projects ProFI (Proteomics French Infrastructure, ANR-10-INBS-08) and GRAL, a program from the Chemistry Biology Health (CBH) Graduate School of University Grenoble Alpes (ANR-17-EURE-0003).

Author contributions

M.B. conducted most of the experiments and contributed to the writing of the manuscript. L.E.K., M.Co. and R.D. designed, performed and/or analyzed RNA-seq experiments. C.G. collected samples, conducted and analyzed experiments. M.Cr., D.P. designed, performed and/or analyzed histone PTMs and variants by proteomics. A.I., C.I-R., C.L., M.G., M.D. and I.S-C. performed and analyzed other experiments. N.V. contributed to data analyses. P.F. and A.Z. contributed to data analyses and

618 provided expertise. K.Y., F.V.L., A.L., R.O. and Y.O. provided resources and expertise. J.C. supervised
619 the project, conducted experiments and wrote the manuscript.

620 **Data availability**

621 RNA-seq data have been submitted to ENA repository under project number PRJEB50887
622 (https://www.ebi.ac.uk/ena/). The mass spectrometry proteomics data have been deposited to the
623 ProteomeXchange Consortium via the PRIDE (Perez-Riverol et al., 2019) partner repository with the
624 dataset identifier PXD030734 and 10.6019/PXD030734.

625

626 **Figure Legend**

627 **Figure 1. DOT1L expression in meiotic and postmeiotic germ cells of *Dot1l*-KO and CTL males**

628 A) Spermatogenesis scheme representing the dynamic of histone to protamine transition. B) Western
629 blot detection of DOT1L and TUBULIN (TUB) in whole testicular protein extracts from CTL and *Dot1l*-
630 KO (KO) adult mice. C) Immunohistochemistry detection of DOT1L in testicular sections from CTL and
631 *Dot1l*-KO (KO) adult mice. SC = Spermatocytes, RS = Round spermatids, ES = Elongating spermatids.
632 Pictures were taken using the same parameters. Scale bars indicate 50µm. D) Western blot detection
633 of DOT1L and H3K79me2 in *Dot1l*-KO (KO) and CTL germ cells. Normalization was performed by
634 detecting the membrane with anti-TUBULIN (TUB). SC = primary spermatocytes, RS = round
635 spermatids. See also Figure S1.

636 **Figure 2. *Dot1l*-KO in male germ cells impairs spermatogenesis and male fertility**

637 A) Scatter plots (mean + standard deviation) showing the average testis weight, body weight and sperm
638 count in *Dot1l*-KO and CTL adult mice (2 to 4 month-old N>10 for CTL and *Dot1l*-KO samples). B)
639 Histology of *Dot1l*-KO and CTL testes (periodic acid-Schiff staining). Scale bars indicate 200µm. C)
640 Schematic diagram representing total number of each cell type per testis in CTL and *Dot1l*-KO males,
641 as calculated by FACS. 4N = Primary spermatocytes, 2N = Secondary spermatocytes, N = spermatids,
642 SP = Side Population representing premeiotic germ cells (spermatogonia). 8 CTL and 6 *Dot1l*-KO testes
643 were analyzed. One or two stars indicate a p-value <0.05 or <0.01, respectively (Student t-test). D)
644 Results from the tests of fertility (natural mating) of *Dot1l*-KO and CTL males (7 males in each group
645 mated for ~3 months with wild-type females). Schematic diagrams representing the number of litters
646 and the litter size from progeny of *Dot1l*-KO or CTL males (mean + standard deviation). E) In Vitro
647 Fertilization results. The percentages of fertilized oocytes are indicated for WT, CTL and HET males ('all
648 CTL') and for *Dot1l*-KO males. The left panel shows results using oocytes with intact cumulus, the right
649 panel shows results using oocytes of which the zona pellucida was removed beforehand. See also
650 Figure S2.

Figure 3. ***Dot1l*-KO in male germ cells leads to multiple spermiogenesis defects including flagellar abnormalities and incomplete sperm chromatin reorganization and compaction**

A) Representative pictures of *Dot1l*-KO and CTL epididymal spermatozoa. The black arrow indicates an abnormal sperm head (without apical hook) and white arrows indicate thinning of the flagellum. Scale bars represent 10µm. B) Ultrastructure pictures (electron microscopy) from epididymal spermatozoa showing multiple abnormalities in *Dot1l*-KO compared to CTL: disorganized microtubules (blue arrow), impaired nuclear compaction (top panels) and increased cytoplasmic retention (bottom right panel). Scale bar indicates 1µm. C) Scatter plots (mean values following angular transformation +/- standard deviation) of the percentage of motile and progressively motile spermatozoa in *Dot1l*-KO and CTL adult mice (N= 12 for CTL and 10 for *Dot1l*-KO) obtained following CASA (computer-assisted sperm analysis). Three stars indicate a p-value <0.0005 (Mann Whitney test performed after angular transformation of the percentages). D) Bar plots showing the percentage of testicular tubules with TUNEL-positive elongating/condensing spermatids (ES) (mean per animal + standard error of the mean, N=5 for CTL and 6 for *Dot1l*-KO). Two stars indicate a p-value <0.005 (unpaired t-test performed after angular transformation of percentages). A representative picture of *Dot1l*-KO testicular sections following TUNEL assay is shown on the right. TUNEL positive elongating/condensing spermatids are visible inside the tubule (in green, white arrowhead). DAPI (blue) was used to stain nuclei. Scale bar indicates 20µm. E) Western blot detection of histones H3 and TH2B in spermatozoa from *Dot1l*-KO and CTL males. The same quantity of material has been loaded in each well (i.e. extracts from 2millions spermatozoa). The right panels show the quantification of histones H3 and TH2B in spermatozoa from 11 CTL and 10 *Dot1l*-KO males (mean + standard error of the mean), all extracted and loaded similarly. One star indicates a p-value <0.05 (unpaired t-test). F) Coomassie-stained protamine extracts from CTL and *Dot1l*-KO spermatozoa following acid urea gel electrophoresis (same gel, two different intensities). The same quantity of material has been loaded in each well (i.e. extracts from 1.4millions spermatozoa). Protamine 1 and 2 bands (PRM1 and PRM2, respectively) are detected at the bottom of the gel, while immature forms of Protamine 2 (i.e. non-cleaved forms) are shown in the rectangle. The right panel shows the quantification of PRM1/PRM2 ratio following acid urea gel electrophoresis. One star indicates a p-value <0.05 (unpaired t-test). A.U. = arbitrary units. See also Figure S3.

Figure 4. *Dot1l*-KO extensively modifies the chromatin of elongating spermatids

Bar plots showing the quantification of post-translational modifications (PTMs) in histones H3 and H4 in ES (elongating/condensing spermatids) by mass spectrometry. After normalization to be at constant amount of histone H3 or H4 in each analyzed sample (see Material and methods), mass spectrometry signals were divided by the average signal in both conditions (CTL and KO), so as to be able to represent

all peptides in the same figure, whatever their MS intensity. Error bars represent standard deviations calculated on the measurements made on biological replicates (N= 3 CTL and 4 KO). When interpreting our mass spectrometry data against the database MS_histoneDB, we were able to identify various H3 variants, namely canonical H3 and variants H3.3, testis-specific H3t and H3mm13. "H3" indicates sequences shared among several variants; "H3.3", "H3t" or "H3mm13", each variant. See also Figure S4.

Figure 5. *Dot1l*-KO leads to the regulation of >1000 genes involved in various biological processes, in particular transcription regulation, chromatin organization, mitochondria function and apoptosis.

A and B) DESeq2 analysis of *Dot1l*-KO vs CTL RNA-seq. A) Multi-dimensional scaling plot on the 500 most expressed genes using pairwise gene selection. B) Upset graph showing number of genes deregulated in each *Dot1l*-KO cell type (RS: Round spermatids, SCII: Secondary spermatocytes, SC: Primary Spermatocytes) and in common between cell types. C) GSEA analysis of *Dot1l*-KO vs CTL RNA-seq. The figures show all the significant biological pathways found significantly downregulated in *Dot1l*-KO round spermatids ($p<0.05$), ranked by their enrichment score. The legend indicates the color code (in grey, "other" pathways). See also Figure S5.

Supplemental Material

Fig. S1: Complement to Figure 1

Fig. S2: Complement to Figure 2

Fig. S3: Complement to Figure 3

Fig. S4: Complement to Figure 4

Fig. S5: Complement to Figure 5

Table S1: Primers

Table S2: Antibody references and usage

References

Aguilar, D., J. Strom, and Q.M. Chen. 2014. Glucocorticoid induced leucine zipper inhibits apoptosis of cardiomyocytes by doxorubicin. *Toxicol Appl Pharmacol*. 276:55-62.

Ahmed, E.A., and D.G. de Rooij. 2009. Staging of mouse seminiferous tubule cross-sections. *Methods Mol Biol*. 558:263-277.

Bao, J., and M.T. Bedford. 2016. Epigenetic regulation of the histone-to-protamine transition during spermiogenesis. *Reproduction (Cambridge, England)*. 151:R55-70.

Bao, J., H.Y. Ma, A. Schuster, Y.M. Lin, and W. Yan. 2013. Incomplete cre-mediated excision leads to phenotypic differences between Stra8-iCre; Mov10l1(lox/lox) and Stra8-iCre; Mov10l1(lox/Delta) mice. *Genesis*. 51:481-490.

Barral, S., Y. Morozumi, H. Tanaka, E. Montellier, J. Govin, M. de Dieuleveult, G. Charbonnier, Y. Coute, D. Puthier, T. Buchou, F. Boussouar, T. Urahama, F. Fenaille, S. Curtet, P. Hery, N. Fernandez-

Nunez, H. Shiota, M. Gerard, S. Rousseaux, H. Kurumizaka, and S. Khochbin. 2017. Histone Variant H2A.L.2 Guides Transition Protein-Dependent Protamine Assembly in Male Germ Cells. *Mol Cell*. 66:89-101 e108.

Bouyssie, D., A.M. Hesse, E. Mouton-Barbosa, M. Rompais, C. Macron, C. Carapito, A. Gonzalez de Peredo, Y. Coute, V. Dupierris, A. Burel, J.P. Menetrey, A. Kalaitzakis, J. Poisat, A. Romdhani, O. Burlet-Schiltz, S. Cianferani, J. Garin, and C. Bruley. 2020. Proline: an efficient and user-friendly software suite for large-scale proteomics. *Bioinformatics*. 36:3148-3155.

Braun, R.E. 2001. Packaging paternal chromosomes with protamine. *Nature genetics*. 28:10-12.

Bu, J., A. Chen, X. Yan, F. He, Y. Dong, Y. Zhou, J. He, D. Zhan, P. Lin, Y. Hayashi, Y. Sun, Y. Zhang, Z. Xiao, H.L. Grimes, Q.F. Wang, and G. Huang. 2018. SETD2-mediated crosstalk between H3K36me3 and H3K79me2 in MLL-rearranged leukemia. *Leukemia*. 32:890-899.

Chen, Y., Y. Zheng, Y. Gao, Z. Lin, S. Yang, T. Wang, Q. Wang, N. Xie, R. Hua, M. Liu, J. Sha, M.D. Griswold, J. Li, F. Tang, and M.H. Tong. 2018. Single-cell RNA-seq uncovers dynamic processes and critical regulators in mouse spermatogenesis. *Cell Res*. 28:879-896.

Cocquet, J., P.J. Ellis, Y. Yamauchi, S.K. Mahadevaiah, N.A. Affara, M.A. Ward, and P.S. Burgoyne. 2009. The multicopy gene Sly represses the sex chromosomes in the male mouse germline after meiosis. *PLoS biology*. 7:e1000244.

Comptour, A., C. Moretti, M.E. Serrentino, J. Auer, C. Ialy-Radio, M.A. Ward, A. Toure, D. Vaiman, and J. Cocquet. 2014. SSTY proteins co-localize with the post-meiotic sex chromatin and interact with regulators of its expression. *The FEBS journal*. 281:1571-1584.

Corbineau, S., B. Lassalle, M. Givelet, I. Souissi-Sarahoui, V. Firlej, P.H. Romeo, I. Allemand, L. Riou, and P. Fouchet. 2017. Spermatogonial stem cells and progenitors are refractory to reprogramming to pluripotency by the transcription factors Oct3/4, c-Myc, Sox2 and Klf4. *Oncotarget*. 8:10050-10063.

Crespo, M., A. Damont, M. Blanco, E. Lastrucci, S.E. Kennani, C. Ialy-Radio, L.E. Khattabi, S. Terrier, M. Louwagie, S. Kieffer-Jaquinod, A.M. Hesse, C. Bruley, S. Chantalat, J. Govin, F. Fenaille, C. Battail, J. Cocquet, and D. Pflieger. 2020. Multi-omic analysis of gametogenesis reveals a novel signature at the promoters and distal enhancers of active genes. *Nucleic Acids Res*. 48:4115-4138.

da Cruz, I., R. Rodriguez-Casuriaga, F.F. Santinaque, J. Farias, G. Curti, C.A. Capoano, G.A. Folle, R. Benavente, J.R. Sotelo-Silveira, and A. Geisinger. 2016. Transcriptome analysis of highly purified mouse spermatogenic cell populations: gene expression signatures switch from meiotic-to postmeiotic-related processes at pachytene stage. *BMC genomics*. 17:294.

Dobin, A., and T.R. Gingeras. 2015. Mapping RNA-seq Reads with STAR. *Curr Protoc Bioinformatics*. 51:11 14 11-19.

Dong, Y., K.I. Isono, K. Ohbo, T.A. Endo, O. Ohara, M. Maekawa, Y. Toyama, C. Ito, K. Toshimori, K. Helin, N. Ogonuki, K. Inoue, A. Ogura, K. Yamagata, I. Kitabayashi, and H. Koseki. 2017. EPC1/TIP60-Mediated Histone Acetylation Facilitates Spermiogenesis in Mice. *Mol Cell Biol*. 37.

Dottermusch-Heidel, C., S.M. Gartner, I. Tegeder, C. Rathke, B. Barckmann, M. Bartkuhn, S. Bhushan, K. Steger, A. Meinhardt, and R. Renkawitz-Pohl. 2014a. H3K79 methylation: a new conserved mark that accompanies H4 hyperacetylation prior to histone-to-protamine transition in Drosophila and rat. *Biol Open*. 3:444-452.

Dottermusch-Heidel, C., E.S. Klaus, N.H. Gonzalez, S. Bhushan, A. Meinhardt, M. Bergmann, R. Renkawitz-Pohl, C. Rathke, and K. Steger. 2014b. H3K79 methylation directly precedes the histone-to-protamine transition in mammalian spermatids and is sensitive to bacterial infections. *Andrology*. 2:655-665.

Durinck, S., Y. Moreau, A. Kasprzyk, S. Davis, B. De Moor, A. Brazma, and W. Huber. 2005. BioMart and Bioconductor: a powerful link between biological databases and microarray data analysis. *Bioinformatics*. 21:3439-3440.

El Kennani, S., A. Adrait, A.K. Shaytan, S. Khochbin, C. Bruley, A.R. Panchenko, D. Landsman, D. Pflieger, and J. Govin. 2017. MS_HistoneDB, a manually curated resource for proteomic analysis of human and mouse histones. *Epigenetics Chromatin*. 10:2.

772 Ernst, C., N. Eling, C.P. Martinez-Jimenez, J.C. Marioni, and D.T. Odom. 2019. Staged developmental
773 mapping and X chromosome transcriptional dynamics during mouse spermatogenesis. *Nature*
774 *communications*. 10:1251.
775 Frehlick, L.J., J.M. Eirin-Lopez, and J. Ausio. 2007. New insights into the nucleophosmin/nucleoplasmin
776 family of nuclear chaperones. *Bioessays*. 29:49-59.
777 Garcia-Rodriguez, A., J. Gosalvez, A. Agarwal, R. Roy, and S. Johnston. 2018. DNA Damage and Repair
778 in Human Reproductive Cells. *Int J Mol Sci*. 20.
779 Gaucher, J., F. Boussouar, E. Montellier, S. Curtet, T. Buchou, S. Bertrand, P. Hery, S. Jounier, A. Depaux,
780 A.L. Vitte, P. Guardiola, K. Pernet, A. Debernardi, F. Lopez, H. Holota, J. Imbert, D.J. Wolgemuth,
781 M. Gerard, S. Rousseaux, and S. Khochbin. 2012. Bromodomain-dependent stage-specific male
782 genome programming by Brdt. *The EMBO journal*. 31:3809-3820.
783 Gilan, O., E.Y. Lam, I. Becher, D. Lugo, E. Cannizzaro, G. Joberty, A. Ward, M. Wiese, C.Y. Fong, S. Ftouni,
784 D. Tyler, K. Stanley, L. MacPherson, C.F. Weng, Y.C. Chan, M. Ghisi, D. Smil, C. Carpenter, P.
785 Brown, N. Garton, M.E. Blewitt, A.J. Bannister, T. Kouzarides, B.J. Huntly, R.W. Johnstone, G.
786 Drewes, S.J. Dawson, C.H. Arrowsmith, P. Grandi, R.K. Prinjha, and M.A. Dawson. 2016.
787 Functional interdependence of BRD4 and DOT1L in MLL leukemia. *Nature structural &*
788 *molecular biology*. 23:673-681.
789 Goudarzi, A., D. Zhang, H. Huang, S. Barral, O.K. Kwon, S. Qi, Z. Tang, T. Buchou, A.L. Vitte, T. He, Z.
790 Cheng, E. Montellier, J. Gaucher, S. Curtet, A. Debernardi, G. Charbonnier, D. Puthier, C.
791 Petosa, D. Panne, S. Rousseaux, R.G. Roeder, Y. Zhao, and S. Khochbin. 2016. Dynamic
792 Competing Histone H4 K5K8 Acetylation and Butyrylation Are Hallmarks of Highly Active Gene
793 Promoters. *Mol Cell*. 62:169-180.
794 Green, C.D., Q. Ma, G.L. Manske, A.N. Shami, X. Zheng, S. Marini, L. Moritz, C. Sultan, S.J. Gurczynski,
795 B.B. Moore, M.D. Tallquist, J.Z. Li, and S.S. Hammoud. 2018. A Comprehensive Roadmap of
796 Murine Spermatogenesis Defined by Single-Cell RNA-Seq. *Developmental cell*. 46:651-667
797 e610.
798 Jo, S.Y., E.M. Granowicz, I. Maillard, D. Thomas, and J.L. Hess. 2011. Requirement for Dot1l in murine
799 postnatal hematopoiesis and leukemogenesis by MLL translocation. *Blood*. 117:4759-4768.
800 Jones, B., H. Su, A. Bhat, H. Lei, J. Bajko, S. Hevi, G.A. Baltus, S. Kadam, H. Zhai, R. Valdez, S. Gonzalo, Y.
801 Zhang, E. Li, and T. Chen. 2008. The histone H3K79 methyltransferase Dot1L is essential for
802 mammalian development and heterochromatin structure. *PLoS Genet*. 4:e1000190.
803 Kim, W., M. Choi, and J.E. Kim. 2014. The histone methyltransferase Dot1/DOT1L as a critical regulator
804 of the cell cycle. *Cell Cycle*. 13:726-738.
805 Koster, J., and S. Rahmann. 2018. Snakemake-a scalable bioinformatics workflow engine.
806 *Bioinformatics*. 34:3600.
807 Kuang, W., J. Zhang, Z. Lan, R. Deepak, C. Liu, Z. Ma, L. Cheng, X. Zhao, X. Meng, W. Wang, X. Wang, L.
808 Xu, Y. Jiao, Q. Luo, Z. Meng, K. Kee, X. Liu, H. Deng, W. Li, H. Fan, and L. Chen. 2021. SLC22A14
809 is a mitochondrial riboflavin transporter required for sperm oxidative phosphorylation and
810 male fertility. *Cell reports*. 35:109025.
811 Kurosu, T., T. Fukuda, T. Miki, and O. Miura. 2003. BCL6 overexpression prevents increase in reactive
812 oxygen species and inhibits apoptosis induced by chemotherapeutic reagents in B-cell
813 lymphoma cells. *Oncogene*. 22:4459-4468.
814 Lin, H., K. Cheng, H. Kubota, Y. Lan, S.S. Riedel, K. Kakiuchi, K. Sasaki, K.M. Bernt, M.S. Bartolomei, M.
815 Luo, and P.J. Wang. 2022. Histone methyltransferase DOT1L is essential for self-renewal of
816 germline stem cells. *Genes & development*. 36:752-763.
817 Lin, Y.H., P.M. Kakadia, Y. Chen, Y.Q. Li, A.J. Deshpande, C. Buske, K.L. Zhang, Y. Zhang, G.L. Xu, and S.K.
818 Bohlander. 2009. Global reduction of the epigenetic H3K79 methylation mark and increased
819 chromosomal instability in CALM-AF10-positive leukemias. *Blood*. 114:651-658.
820 Love, M.I., W. Huber, and S. Anders. 2014. Moderated estimation of fold change and dispersion for
821 RNA-seq data with DESeq2. *Genome biology*. 15:550.

822 Luense, L.J., G. Donahue, E. Lin-Shiao, R. Rangel, A.H. Weller, M.S. Bartolomei, and S.L. Berger. 2019.
823 Gcn5-Mediated Histone Acetylation Governs Nucleosome Dynamics in Spermiogenesis.
824 *Developmental cell*.
825 Luense, L.J., X. Wang, S.B. Schon, A.H. Weller, E. Lin Shiao, J.M. Bryant, M.S. Bartolomei, C. Coutifaris,
826 B.A. Garcia, and S.L. Berger. 2016. Comprehensive analysis of histone post-translational
827 modifications in mouse and human male germ cells. *Epigenetics Chromatin*. 9:24.
828 Maruyama, S.Y., M. Ito, Y. Ikami, Y. Okitsu, C. Ito, K. Toshimori, W. Fujii, and K. Yogo. 2016. A critical
829 role of solute carrier 22a14 in sperm motility and male fertility in mice. *Sci Rep*. 6:36468.
830 Montellier, E., F. Boussouar, S. Rousseaux, K. Zhang, T. Buchou, F. Fenaille, H. Shiota, A. Debernardi, P.
831 Hery, S. Curtet, M. Jamshidikia, S. Barral, H. Holota, A. Bergon, F. Lopez, P. Guardiola, K. Pernet,
832 J. Imbert, C. Petosa, M. Tan, Y. Zhao, M. Gerard, and S. Khochbin. 2013. Chromatin-to-
833 nucleoprotamine transition is controlled by the histone H2B variant TH2B. *Genes &*
834 *development*. 27:1680-1692.
835 Moretti, C., M.E. Serrentino, C. Ialy-Radio, M. Delessard, T.A. Soboleva, F. Tores, M. Leduc, P. Nitschke,
836 J.R. Drevet, D.J. Tremethick, D. Vaiman, A. Kocer, and J. Cocquet. 2017. SLY regulates genes
837 involved in chromatin remodeling and interacts with TBL1XR1 during sperm differentiation.
838 *Cell death and differentiation*. 24:1029-1044.
839 Muzumdar, M.D., B. Tasic, K. Miyamichi, L. Li, and L. Luo. 2007. A global double-fluorescent Cre
840 reporter mouse. *Genesis*. 45:593-605.
841 Nguyen, A.T., O. Taranova, J. He, and Y. Zhang. 2011. DOT1L, the H3K79 methyltransferase, is required
842 for MLL-AF9-mediated leukemogenesis. *Blood*. 117:6912-6922.
843 Okada, Y., Q. Feng, Y. Lin, Q. Jiang, Y. Li, V.M. Coffield, L. Su, G. Xu, and Y. Zhang. 2005. hDOT1L links
844 histone methylation to leukemogenesis. *Cell*. 121:167-178.
845 Oliva, R. 2006. Protamines and male infertility. *Human reproduction update*. 12:417-435.
846 Oliva, R., D. Bazett-Jones, C. Mezquita, and G.H. Dixon. 1987. Factors affecting nucleosome disassembly
847 by protamines in vitro. Histone hyperacetylation and chromatin structure, time dependence,
848 and the size of the sperm nuclear proteins. *The Journal of biological chemistry*. 262:17016-
849 17025.
850 Onder, T.T., N. Kara, A. Cherry, A.U. Sinha, N. Zhu, K.M. Bernt, P. Cahan, B.O. Marcarci, J. Unternaehrer,
851 P.B. Gupta, E.S. Lander, S.A. Armstrong, and G.Q. Daley. 2012. Chromatin-modifying enzymes
852 as modulators of reprogramming. *Nature*. 483:598-602.
853 Perez-Riverol, Y., A. Csordas, J. Bai, M. Bernal-Llinares, S. Hewapathirana, D.J. Kundu, A. Inuganti, J.
854 Griss, G. Mayer, M. Eisenacher, E. Perez, J. Uszkoreit, J. Pfeuffer, T. Sachsenberg, S. Yilmaz, S.
855 Tiwary, J. Cox, E. Audain, M. Walzer, A.F. Jarnuczak, T. Ternent, A. Brazma, and J.A. Vizcaino.
856 2019. The PRIDE database and related tools and resources in 2019: improving support for
857 quantification data. *Nucleic Acids Res*. 47:D442-D450.
858 Ragazzini, R., R. Perez-Palacios, I.H. Baymaz, S. Diop, K. Ancelin, D. Zielinski, A. Michaud, M. Givelet, M.
859 Borsos, S. Aflaki, P. Legoix, P. Jansen, N. Servant, M.E. Torres-Padilla, D. Bourc'his, P. Fouchet,
860 M. Vermeulen, and R. Margueron. 2019. EZHIP constrains Polycomb Repressive Complex 2
861 activity in germ cells. *Nature communications*. 10:3858.
862 Rathke, C., W.M. Baarends, S. Awe, and R. Renkawitz-Pohl. 2014. Chromatin dynamics during
863 spermiogenesis. *Biochim Biophys Acta*. 1839:155-168.
864 Robinson, M.D., D.J. McCarthy, and G.K. Smyth. 2010. edgeR: a Bioconductor package for differential
865 expression analysis of digital gene expression data. *Bioinformatics*. 26:139-140.
866 Sadate-Ngatchou, P.I., C.J. Payne, A.T. Dearth, and R.E. Braun. 2008. Cre recombinase activity specific
867 to postnatal, premeiotic male germ cells in transgenic mice. *Genesis*. 46:738-742.
868 Shang, E., H.D. Nickerson, D. Wen, X. Wang, and D.J. Wolgemuth. 2007. The first bromodomain of Brdt,
869 a testis-specific member of the BET sub-family of double-bromodomain-containing proteins,
870 is essential for male germ cell differentiation. *Development (Cambridge, England)*. 134:3507-
871 3515.
872 Shiota, H., S. Barral, T. Buchou, M. Tan, Y. Coute, G. Charbonnier, N. Reynoird, F. Boussouar, M. Gerard,
873 M. Zhu, L. Bargier, D. Puthier, F. Chuffart, E. Bourova-Flin, S. Picaud, P. Filippakopoulos, A.

874 Goudarzi, Z. Ibrahim, D. Panne, S. Rousseaux, Y. Zhao, and S. Khochbin. 2018. Nut Directs p300-
875 Dependent, Genome-Wide H4 Hyperacetylation in Male Germ Cells. *Cell reports*. 24:3477-
876 3487 e3476.
877 Soler-Ventura, A., J. Castillo, A. de la Iglesia, M. Jodar, F. Barrachina, J.L. Ballesca, and R. Oliva. 2018.
878 Mammalian Sperm Protamine Extraction and Analysis: A Step-By-Step Detailed Protocol and
879 Brief Review of Protamine Alterations. *Protein Pept Lett*. 25:424-433.
880 Soumillon, M., A. Necsulea, M. Weier, D. Brawand, X. Zhang, H. Gu, P. Barthes, M. Kokkinaki, S. Nef, A.
881 Gnirke, M. Dym, B. de Massy, T.S. Mikkelsen, and H. Kaessmann. 2013. Cellular source and
882 mechanisms of high transcriptome complexity in the mammalian testis. *Cell reports*. 3:2179-
883 2190.
884 Steger, D.J., M.I. Lefterova, L. Ying, A.J. Stonestrom, M. Schupp, D. Zhuo, A.L. Vakoc, J.E. Kim, J. Chen,
885 M.A. Lazar, G.A. Blobel, and C.R. Vakoc. 2008. DOT1L/KMT4 recruitment and H3K79
886 methylation are ubiquitously coupled with gene transcription in mammalian cells. *Mol Cell*
887 *Biol*. 28:2825-2839.
888 Subramanian, A., P. Tamayo, V.K. Mootha, S. Mukherjee, B.L. Ebert, M.A. Gillette, A. Paulovich, S.L.
889 Pomeroy, T.R. Golub, E.S. Lander, and J.P. Mesirov. 2005. Gene set enrichment analysis: a
890 knowledge-based approach for interpreting genome-wide expression profiles. *Proceedings of*
891 *the National Academy of Sciences of the United States of America*. 102:15545-15550.
892 Thomis, D.C., W. Lee, and L.J. Berg. 1997. T cells from Jak3-deficient mice have intact TCR signaling, but
893 increased apoptosis. *J Immunol*. 159:4708-4719.
894 Toure, A. 2019. Importance of SLC26 Transmembrane Anion Exchangers in Sperm Post-testicular
895 Maturation and Fertilization Potential. *Front Cell Dev Biol*. 7:230.
896 Valencia-Sanchez, M.I., P. De Ioannes, M. Wang, D.M. Truong, R. Lee, J.P. Armache, J.D. Boeke, and K.J.
897 Armache. 2021. Regulation of the Dot1 histone H3K79 methyltransferase by histone H4K16
898 acetylation. *Science*. 371.
899 Vlaming, H., and F. van Leeuwen. 2016. The upstreams and downstreams of H3K79 methylation by
900 DOT1L. *Chromosoma*.
901 Wang, Z., C. Zang, J.A. Rosenfeld, D.E. Schones, A. Barski, S. Cuddapah, K. Cui, T.Y. Roh, W. Peng, M.Q.
902 Zhang, and K. Zhao. 2008. Combinatorial patterns of histone acetylations and methylations in
903 the human genome. *Nature genetics*. 40:897-903.
904 Ward, W.S., and D.S. Coffey. 1991. DNA packaging and organization in mammalian spermatozoa:
905 comparison with somatic cells. *Biology of reproduction*. 44:569-574.
906 Yamaguchi, K., M. Hada, Y. Fukuda, E. Inoue, Y. Makino, Y. Katou, K. Shirahige, and Y. Okada. 2018. Re-
907 evaluating the Localization of Sperm-Retained Histones Revealed the Modification-Dependent
908 Accumulation in Specific Genome Regions. *Cell reports*. 23:3920-3932.
909 Yamauchi, Y., J.M. Riel, Z. Stoytcheva, P.S. Burgoyne, and M.A. Ward. 2010. Deficiency in mouse Y
910 chromosome long arm gene complement is associated with sperm DNA damage. *Genome*
911 *biology*. 11:R66.
912 Yu, Y.E., Y. Zhang, E. Unni, C.R. Shirley, J.M. Deng, L.D. Russell, M.M. Weil, R.R. Behringer, and M.L.
913 Meistrich. 2000. Abnormal spermatogenesis and reduced fertility in transition nuclear protein
914 1-deficient mice. *Proceedings of the National Academy of Sciences of the United States of*
915 *America*. 97:4683-4688.
916 Zhang, W., Y. Hayashizaki, and B.C. Kone. 2004. Structure and regulation of the mDot1 gene, a mouse
917 histone H3 methyltransferase. *The Biochemical journal*. 377:641-651.
918 Zhu, B., S. Chen, H. Wang, C. Yin, C. Han, C. Peng, Z. Liu, L. Wan, X. Zhang, J. Zhang, C.G. Lian, P. Ma,
919 Z.X. Xu, S. Prince, T. Wang, X. Gao, Y. Shi, D. Liu, M. Liu, W. Wei, Z. Wei, J. Pan, Y. Wang, Z.
920 Xuan, J. Hess, N.K. Hayward, C.R. Goding, X. Chen, J. Zhou, and R. Cui. 2018. The protective role
921 of DOT1L in UV-induced melanomagenesis. *Nature communications*. 9:259.
922
923

Fig1

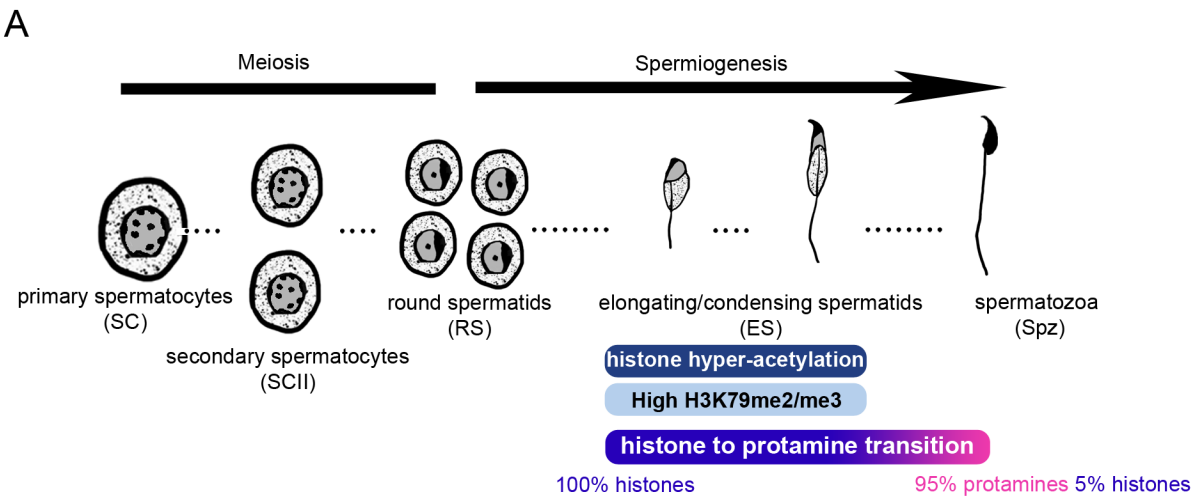

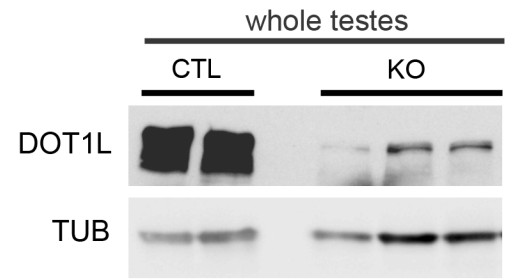

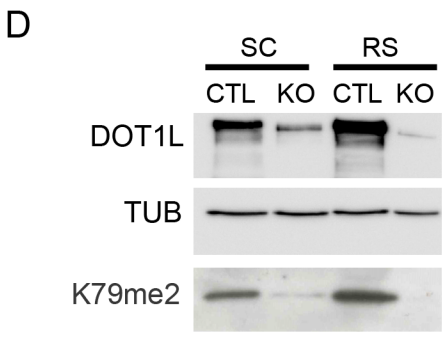

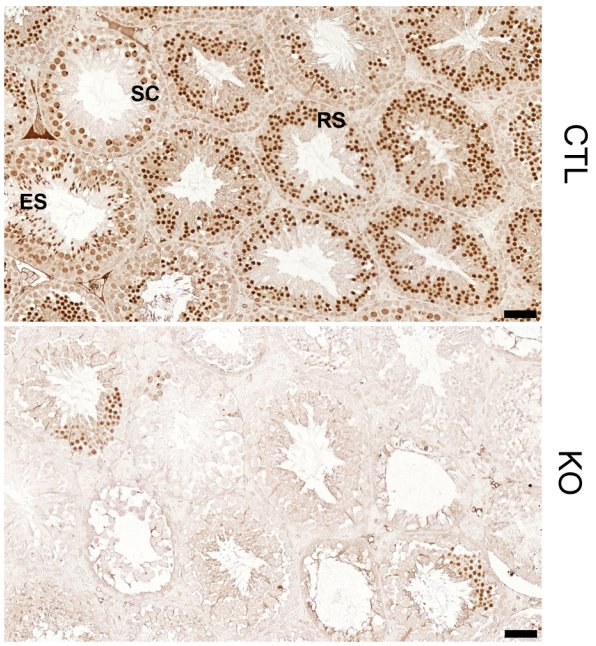

Fig. 2

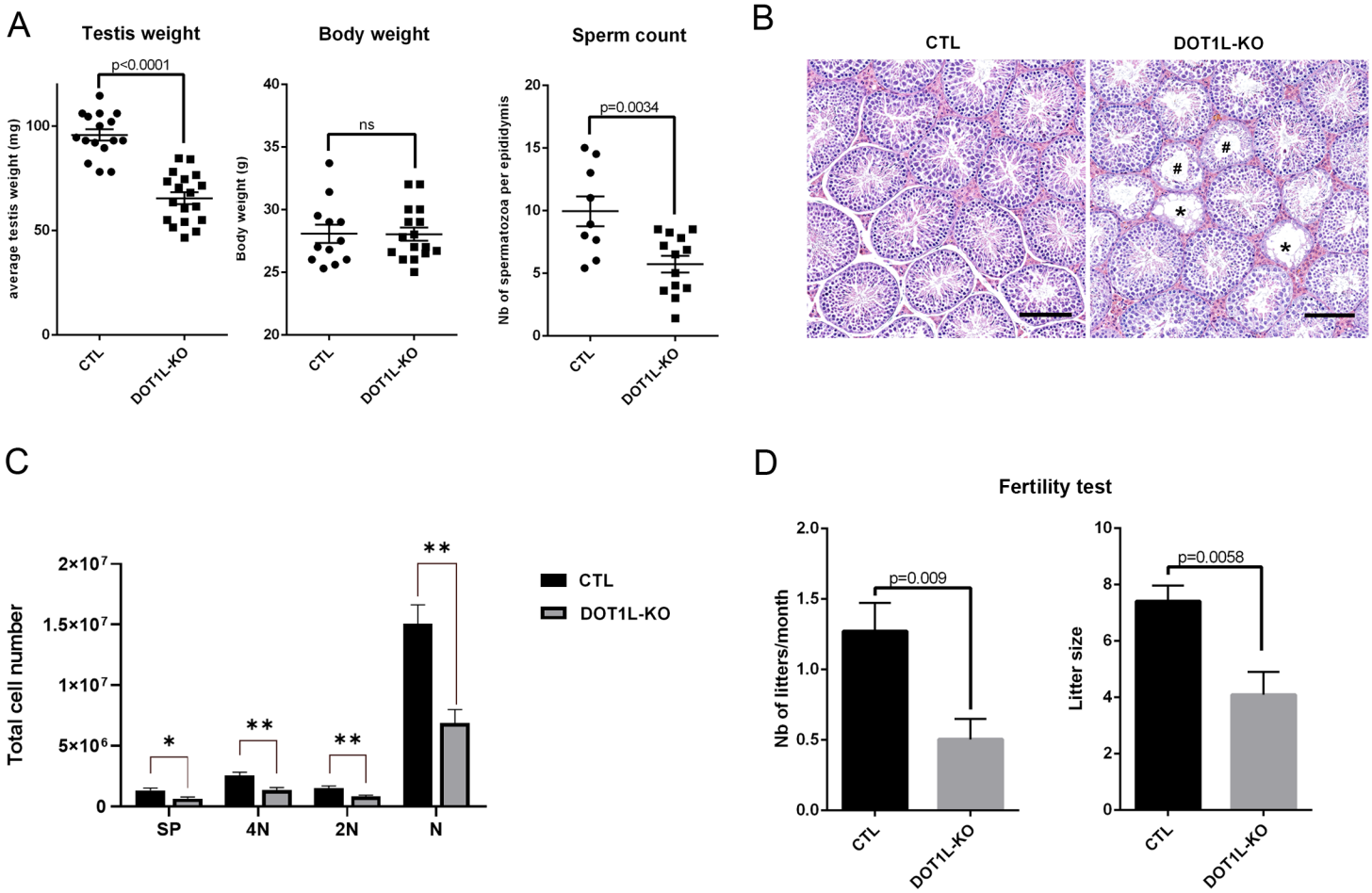

Fig. 3

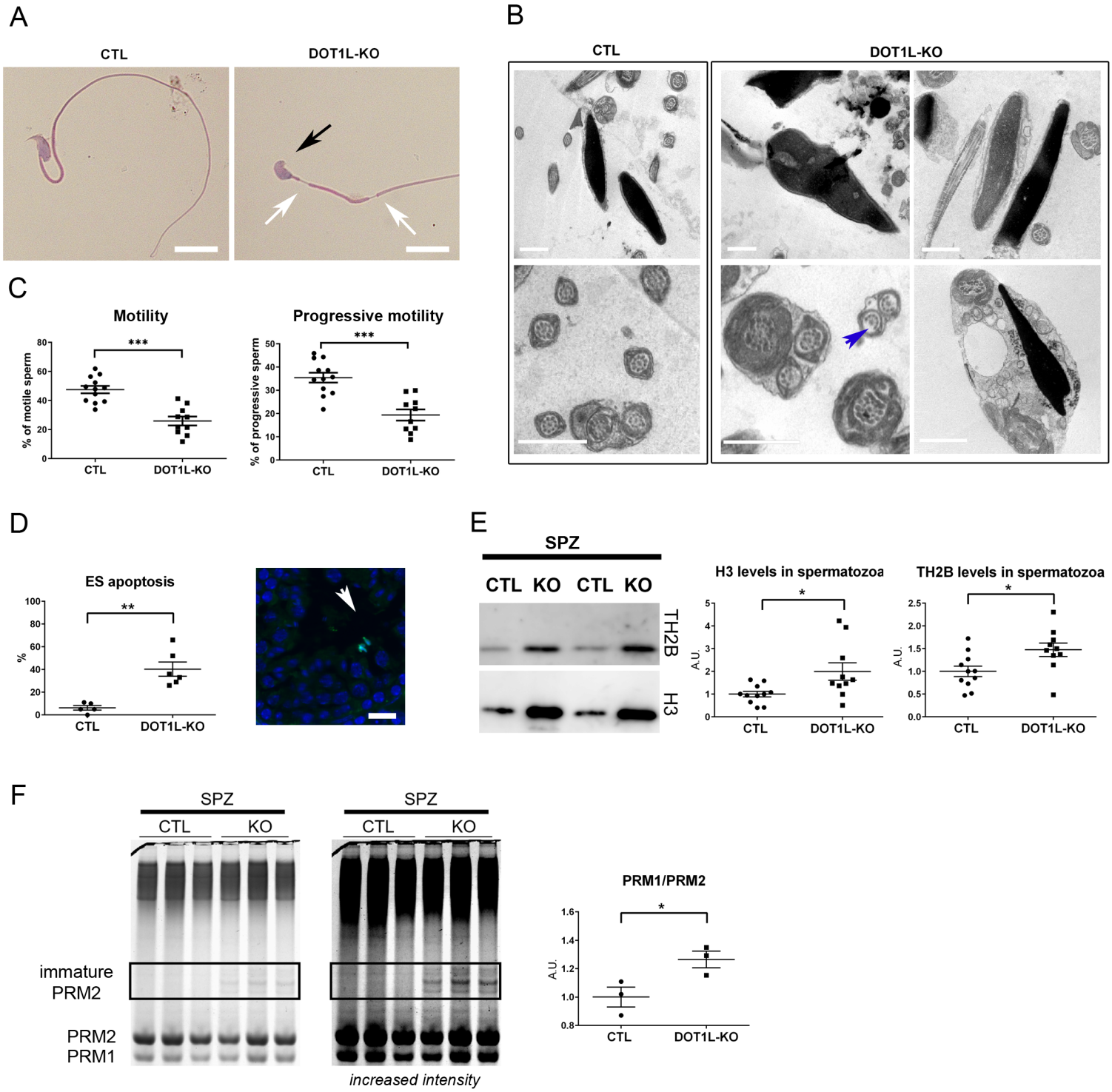

Fig. 4

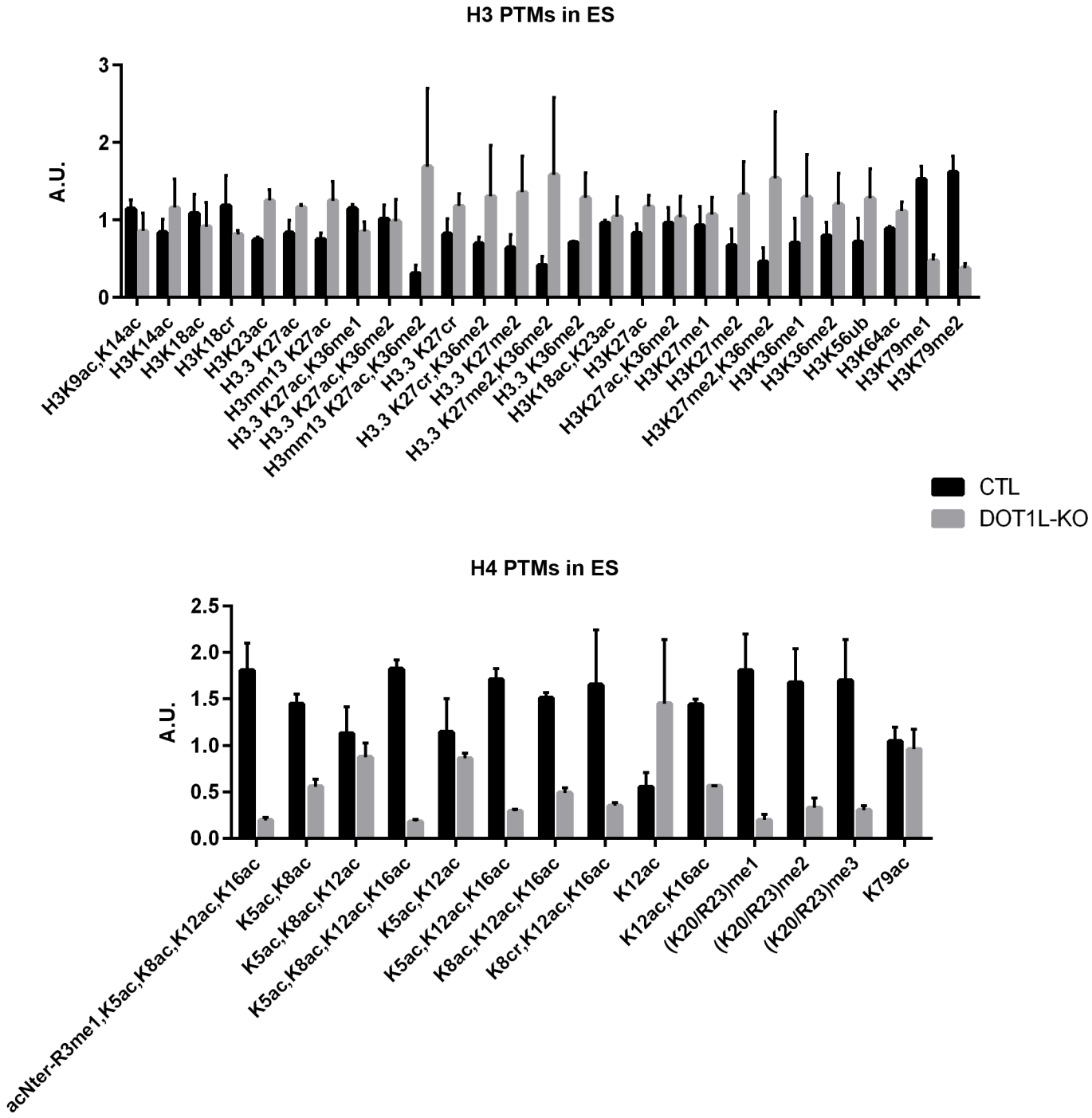

Fig. 5

A

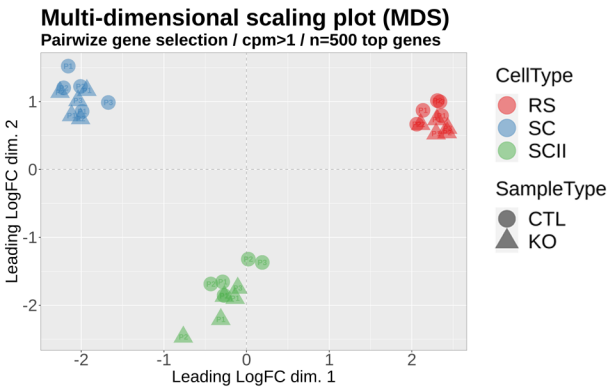

B

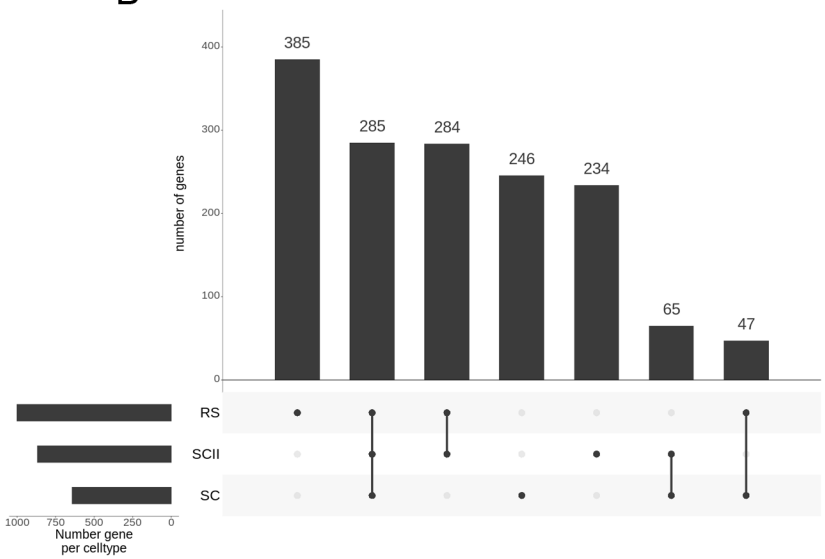

C